Biophysical Chemistry 180–181 (2013) 37–43

Contents lists available at ScienceDirect

Biophysical Chemistry

journal homepage: http://www.elsevier.com/locate/biophyschem

P130Cas substrate domain is intrinsically disordered as characterized by single-molecule force measurements

Chen Lu [a,b,c,1], Fei Wu [a,b,1], Wu Qiu [b], Ruchuan Liu [a,b,c,*]

[a] College of Physics, Chongqing University, No. 55 Daxuecheng South Road, Shapingba District, Chongqing 401331, China
[b] Department of Physics, National University of Singapore, 2 Science Drive 3 117551, Singapore
[c] Mechanobiology Institute, National University of Singapore, 5A Engineering Drive 1 117411, Singapore

HIGHLIGHTS

- Stretching of individual CasSD domains by AFM and magnetic tweezers
- CasSD domains are intrinsically disordered with many native conformations.
- These conformations of CasSD only have limited mechanical stability.
- The stable conformations may be governed by similar weak interactions.
- CasSD is a molecular mechano-sensor for extension changes rather than forces.

GRAPHICAL ABSTRACT

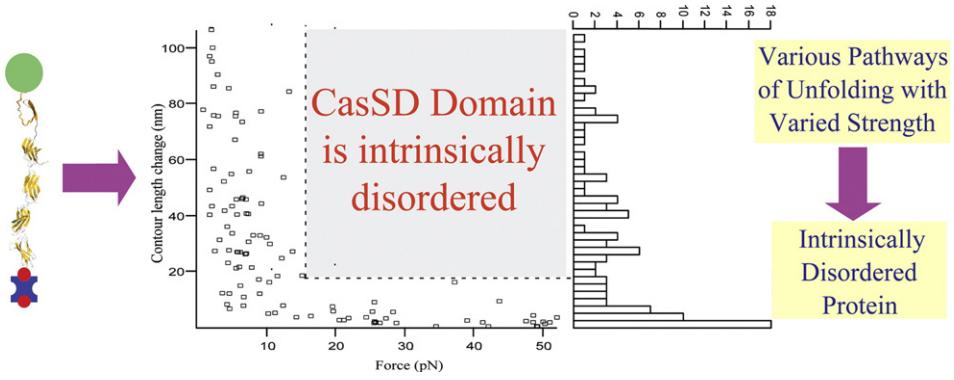

ARTICLE INFO

Article history:
Received 2 May 2013
Received in revised form 9 June 2013
Accepted 11 June 2013
Available online 18 June 2013

Keywords:
p130Cas
Mechano-transduction
AFM
Magnetic tweezer
Intrinsically disordered protein
Tyrosine phosphorylation

ABSTRACT

P130Cas is a docking protein essentially coordinating tyrosine-kinase-based signaling pathways associated with cell adhesion and migration etc. Its central substrate domain (CasSD) can bind to Crk and includes 15 YxxP motifs, where most tyrosine phosphorylation happens. It has been shown that CasSD can be stretched to promote phosphorylation, the mechanism of which needs to be explored in detail. Thus, it is important to uncover the native structure(s) of CasSD and the structural changes associated with mechanical stretching, both of which are still unclear. Here, we used atomic force microscopy force mode and magnetic tweezers to stretch individual molecules of CasSD constructs. Our results showed that the CasSD domain was intrinsically disordered. Natively, CasSD domains took many conformations beside random coils, while most of these conformations possessed limited mechanical stability. In magnetic tweezers experiments, the intramolecular interactions stabilizing the varied native conformations of CasSD were found similar in strength. Such diversity in native conformations of CasSD domains, as discovered here, should play important role in their signaling functions and their limited strength should be relevant to the mechanical activation of those signaling pathways.

* Corresponding author at: College of Physics, Chongqing University, No. 55 Daxuecheng South Road, Shapingba District, Chongqing 401331, China. Tel.: +86 13638370036; fax: +86 23 65678362.
E-mail address: phyliurc@cqu.edu.cn (R. Liu).
[1] Both authors contributed to this paper equally.

0301-4622/$ – see front matter © 2013 Elsevier B.V. All rights reserved.
http://dx.doi.org/10.1016/j.bpc.2013.06.008

1. Introduction

Crk-associated substrate (p130Cas) is a scaffolding protein centering in cellular focal adhesion functions [1–3]. It is the substrate of v-Src family kinases, essential for tyrosine-kinase-based signaling processes. P130Cas is believed to be involved in cell adhesion, migration, transformation, apoptosis, growth factor stimulation, cytokine receptor engagement, bacterial infection, cancer cell invasiveness and resistance to antiestrogenic drugs [4–10]. P130Cas contains multiple conserved protein–protein interaction domains. They are an N-terminal Src homology 3 (SH3) domain that interacts with focal adhesion kinases (FAK) and Dock180 etc. [11], a central substrate domain (CasSD), a Src-binding domain (SBD), and a conserved C-terminal Cas-family homology (CCH) domain [10,12,13]. Both terminal SH3 and CCH domains act as anchor points to localize p130Cas to focal adhesions (FAs) [3], while the CasSD can bind to Crk to activate signaling events [14–16] and SBD domains can also be associated with some biochemical signal initiations [17].

Here, tyrosine phosphorylation is a biochemical pathway to recruit downstream effectors in the signal events. The majority of tyrosine phosphorylation takes place at the 15 YxxP motifs of the CasSD domain. For example, adaptor protein Crk and growth factor like EGF receptor phosphorylate some of those tyrosine residues, thus creating binding sites for SH2 and PTB domains of downstream effectors in the various signaling pathways. Interestingly, Sawada et al. showed that upon cell stretching, the mechanical extension of CasSD can make those YxxP motifs more accessible to phosphorylation [2]. Thus, p130Cas as a force-sensing protein was firstly demonstrated in experiments, and CasSD was the primary region responsible for converting mechanical signals into chemical ones, resembling that of talin rods [18]. However, how it unravels under force to expose tyrosine phosphorylation sites still remains elusive. Even its native structure(s) is still unavailable. On the other hand, multiple growth factors, hormones, kinases/phosphorylases have been shown to regulate CasSD phosphorylation [12]. Whether the regulation by any of these or other factors can be related to consequent changes in CasSD's mechanical property is an important and interesting biophysical question. Therefore, the understanding of the structure and mechanical property of CasSD is essential, but to our knowledge, related study has not been reported yet.

In this work, we present an investigation of the forced unfolding of CasSD using single molecule force techniques, i.e. the force mode of atomic force microscopy (AFM) and magnetic tweezers (MT). Here, the low force capability of the MT can mimic the condition of stretching during cell spreading, so we are able to approach the structural information of CasSD and its mechanical response. As a result, CasSD mainly takes conformation of random coil, while many other mechanically stable conformations coexist. Most of those conformations of CasSD possess limited mechanical stability, and can be unraveled at a low force around 5 pN at an unfolding rate of ~0.13 s^{-1}. All evidences here strongly suggest that CasSD be an intrinsically disordered (ID) domain. Comparing it with those highly established ID protein, we speculate that phosphorylation and change of local ionic strength may provide mechanisms *in vivo* to shift its mechanical property, change the accessibility of tyrosine residues and thus regulate the following signaling pathways.

2. Materials and methods

2.1. CasSD recombinant protein expression and purification

Two types of chimeric proteins of mouse p130Cas substrate domain 115–420 (CasSD), one with I27 and the other with fibronectin type III domain 7–10 ($FnIII_{7-10}$), were expressed in *Escherichia coli* BL21(DE3) Rosetta2 strain (Merck Biosciences, Darmstadt, Germany), with a His_6-tag on the C-terminal of both proteins and an avi-tag on the N-terminal of the CasSD–$FnIII_{7-10}$ fusion protein. Cells were incubated at 37 °C for 3 h in ITPG-added LB culture for gene expression, followed by sonication of the cell suspension in 50 mM potassium phosphate pH 7.8, 300 mM KCl, protease inhibitor cocktail VII (Merck Biosciences, Darmstadt, Germany) lysis buffer and centrifugation. Recombinant protein was purified from cell lysate by cobalt-affinity chromatography using HisPur cobalt resin (Thermo Scientific Pierce Protein Research Products, Rockford, IL). The elution from resin was obtained with 50 mM imidazole. PD-10 desalting column (GE Healthcare, Waukesha, WI) was then used to achieve 1.5 mg/mL target protein in a buffer containing 10 mM potassium phosphate pH 7.5, 100 mM KCl, 1 mM EDTA and 5% (v/v) glycerol, which is subjected to gel-filtration chromatography using a Superdex 10/300 GL column on an ÅKTA purifier liquid chromatography system (GE Healthcare, Waukesha, WI). The purity of the recombinant proteins is final-checked by SDS-polyacrylamide gel electrophoresis (PAGE).

In vitro biotination of the CasSD $FnIII_{7-10}$ was achieved by incubation of purified proteins with 0.2 μM BirA (Avidity, CO) in a solution of 50 mM Bicine–NaOH pH 8.3, 10 mM ATP, 10 mM magnesium acetate, 50 μM D-biotin, 0.1 mM β-mercaptoethanol, 0.1 mM PMSF, 0.1 μg/mL aprotinin, and 0.1 μg/mL leupeptin, at 25 °C for 14 h.

2.2. Substrate and bead modification

Substrates were cleaned before any chemical modification. In details, both glass (Deckglaser, Germany) and quartz (UQG Optics, UK) slides underwent sonication in ethanol for 30 min, followed by incubation in the mixture of H_2O_2 and H_2SO_4 (3:7 in volume) at 100 °C for 1 h. Then, the slides were sonicated sequentially in 1 M NaOH and water for 20 min each. Silanization of slides was carried out in a solution of 1% propylmethyldimethoxysilane (Alfa Aesar, MA), 4% water, and 95% ethanol for 15 min. Finally, two types of surface modification were done by further chemical treatments of the slides. Ni^{2+}–NTA glass slides were obtained by incubation sequentially in 0.05% glutaraldehyde (Sigma Aldrich, MO) solution for 1 h, in 1 μg/mL nitrilotriacetic acid (NTA) (Sigma Aldrich, MO) for 30 min and in 100 mM $NiSO_4$ (Alfa Aesar, MA) solution for 1 h. Biotinylated quartz slides were obtained by incubation in a mixed solution of 5 mM methyl-PEG-SVA (Laysan Bio, AL), 5 nM Biotin-PEG-SVA (Laysan Bio, AL) and 10 mM HEPES for 4 h.

Before MT experiments, biotinylated quartz slides were further incubated with a mixture of 0.2 μg/mL neutravidin (Thermo, IL) and 0.2 μg/mL Cas–fibronectin solutions at a molar ratio of 1:1 for 30 min [19]; then, in MT experiments, incubated with Ni^{2+}–NTA coated green-fluorescent beads. To prepare Ni^{2+}–NTA coated bead, dragon green-fluorescent carboxylic group-covered magnetic bead (Bangs, IN) with a diameter of 2.8 μm were treated with both 50 mg/mL Sulfo-NHS (Alfa Aesar, MA) and 50 mg/mL EDC (Thermo, IL) in 50 mM MES (pH 4.7). After 20 min agitation at room temperature, beads were washed with 50 mM HEPES (pH 7.2), and incubated with 1 μg/mL NTA for 4 h. Then another cycle of wash was carried out, followed by chelation in a 100 mM NiSO4 (Sigma, MO) solution for 1 h and further incubation in a 2 mg/mL BSA solution.

2.3. AFM experiment

Protein stretching experiment under a high loading rate was conducted on a commercial AFM (Veeco, Plainview, NY) in a buffer of 125 mM sodium chloride, 25 mM HEPES, and pH 7.4. Before AFM pulling experiments, ~20 μL of the protein solution (~10 μg/mL) was deposited on Ni^{2+}–NTA glass slides for 15 min, and then 1 mL of the buffer solution was added. In each stretching cycle, the gold coated cantilever (HYDRA2R-100NGG, Appnano Santa Clara, CA) approached and was pushed against the surface at 800 pN for 2 s, followed by withdrawn from the substrate. The approaching and withdrawing of the cantilever were controlled at a constant velocity of

600 nm/s. The AFM results were analyzed by home-written programs in Labview. Unfolding trajectories were fitted with the Worm-Like-Chain Model [20,21]:

$$\frac{Fp}{k_BT}=\frac{1}{4}\left(1-\frac{x}{L_0}\right)^{-2}-\frac{1}{4}+\frac{x}{L_0} \quad (1)$$

where F is the force, T is the room temperature, p the persistent length, x is the extension and L_0 is the contour length of the molecule. The persistence length and the contour length are adjustable during fitting. Then the contour length changes (ΔL) are calculated from consequent unfolding events.

2.4. Magnetic tweezer experiment

Magnetic tweezers/evanescent nanometry [22] was used to investigate the mechanical response of CasSD to forces of ~5 pN, as shown in Fig. 1. A recombinant protein consisting of CasSD and fibronectin type III domain 7–10 ($FnIII_{7-10}$) (Fig. 4a) was expressed and linked to a fluorescent magnetic bead through the His_6–Ni^{2+}–NTA interaction and to a quartz substrate through biotin–avidin–biotin bonds at its terminuses. $FnIII_{7-10}$ served as a spacer to keep the magnetic bead away from the quartz surface upon stretching, resulting in the suppression of non-specific interactions between them. A slow current ramp was applied in a home-made electromagnetic tweezers, ranging from 0 A to 20 A over a timespan of ~10 min. Accordingly, the force applied to the protein molecule increased slowly at a rate of 0.01 pN/s ~ 0.1 pN/s. During the force ramp, the extension of the molecule, equivalent to the bead-surface distance, was monitored via the fluorescence intensity of the bead by a EMCCD camera (QuantEM 512sc, Tucson, AZ) in the evanescent field created by an IX71 total internal fluorescence (TIRF) microscopy (Olympus, Japan) [22]. Trajectories of the extension in staircase manner indicate unfolding of the protein modules in steps. From the electric current recorded for each unfolding step, the unfolding force was calculated according to the force calibration for beads (Supplementary materials), and subsequently, WLC model with the persistence length achieved from AFM results fitting (0.53 nm, Supplementary materials) was applied to retrieve the ΔL from the unfolding step size.

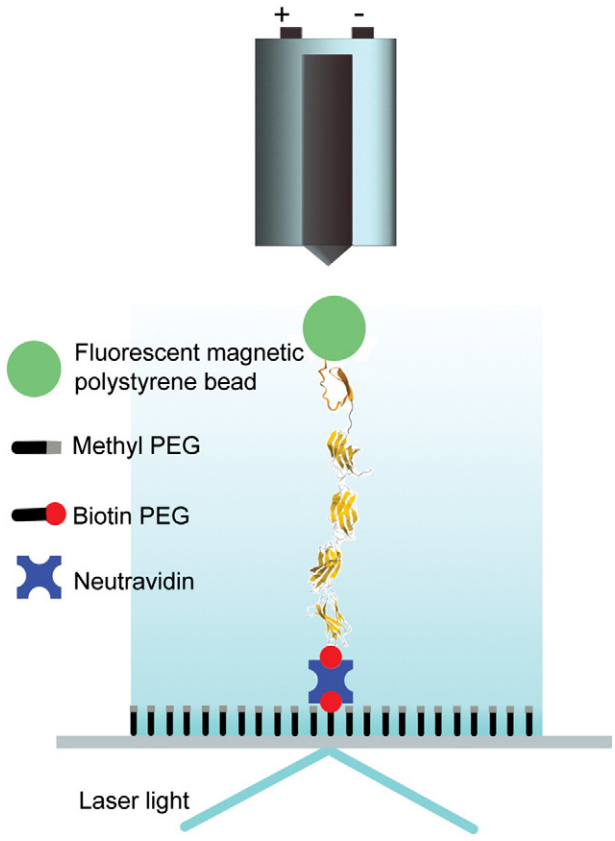

Fig. 1. Scheme of electromagnetic tweezer/evanescent field. Details were described previously [30]. Generally a single protein molecule was linked between a fluorescent magnetic bead and a PEG-passivated quartz surface through the Ni^{2+}–His-tag and biotin–neutravidin conjugations. The paramagnetic bead was lifted upwards in magnetic field as controlled by the current running through the magnetic tweezers. An evanescent field was generated above the quartz surface from total internal reflection of the laser beam at the quartz–water interface. The fluorescence of beads was excited in the evanescent field, with its intensity monitored and correlated to the bead's axial position.

3. Results

3.1. Unfolding CasSD by AFM reveals random unfolding behavior

To unfold CasSD by AFM, a chimeric construct of His_6–$(CasSD\text{-}I27)_2$ was used, in which the His_6-tag can act as the binding site for Ni^{2+}–NTA on the substrates (Fig. 2a). Two I27 domains provide a pair of unfolding peaks (ΔL ~ 28 nm) in the force-versus-extension trajectories as the signature of pulling the right molecule. Any force peak within the same trajectory, other than the two I27 unfolding peaks, is presumably resulted from unfolding CasSD domains. At least, one of the two CasSD domains is flanked at each side by an I27 domain, so it can be sure that this CasSD should be stretched if the two I27 modules are unfolded, no matter where the AFM cantilever may pick up the target protein.

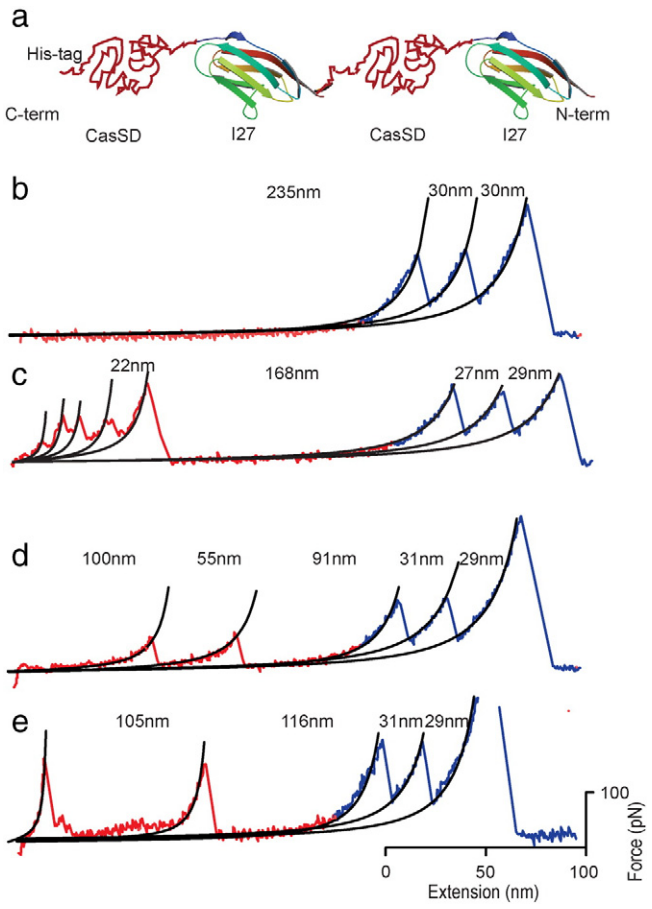

Fig. 2. Unfolding CasSD-I27 recombinant protein using AFM. (a) A scheme of the His_6–$(CasSD\text{-}I27)_2$ protein construct. As one CasSD was adjacent to one I27 domain at each side, only those trajectories with two successive ~28 nm unfolding peaks were picked for unfolding-CasSD analysis. (b) 58% of such curves show no unfolding peaks from CasSD region. The rest 42% of the curves show one (e) or many peaks (c) (d) from CasSD region. Various unfolding patterns were discovered among the unfolding trajectories.

Fig. 2b to e shows some representative trajectories, where the last two unfolding force peaks are attributed to the I27 signature. Because, I27 domain is mechanically more stable, its unfolding force peak can be identified by the higher force and the right ΔL (~28 nm) and unfolding of CasSD should take place before I27 domains in the force–extension trajectories. Among all unfolding trajectories, 75 curves showed two successive I27 peaks, were identified as stretching individual target proteins. Out of them, 43 (~58%) show no unfolding peaks before two I27 ones, indicating that CasSD, in these cases, either has no mechanical strength or unfolds at forces too small to be detected by AFM (Fig. 2b). The rest of the trajectories show up to four unfolding peaks of the CasSD domain (Fig. 2c to e). Furthermore, most target proteins extended to around 250 nm before I27 domains were unfolded. This matches the contour length of the construct under stretching: two CasSD (118.5 nm each, given ~329 amino acids for a CasSD plus the linker and 0.36 nm contour length per peptide) plus the size of two native I27 domains, ~9 nm [23]. Such agreement further confirms that the trajectories came from the right target molecules, and the patterns (unfolding peaks or no any peaks) before the two I27 peaks corresponded to unfolding of CasSD domains.

The AFM results indicate that the CasSD domains take diverse conformations with varied stability. Only less than half (~42%) of these conformations are mechanically stable enough, and unfolding of them results in force peaks in the force–extension trajectories (Fig. 2), among which significant diversity can be found. Even in trajectories with the same number of unfolding steps, the unfolding patterns are not similar to each other. Interestingly, though two CasSD could be unraveled each time, most trajectories didn't show any repetitive unfolding pattern similar to unfolding of poly-I27 [24] and poly-ubiquitin [25]. There is only one trajectory (Fig. 2e), in which both CasSD domains fully unfolded in a single step. The variation in conformation is clearer in the histograms of ΔL and unfolding forces (Fig. 3). The distribution of ΔL (Fig. 3a) is quite broad, ranged over 100 nm from a few nanometers to the contour length of a full CasSD domain, and also random with no characteristic population preference similar to the mechanically stable proteins. In most cases, the ΔL was smaller than that of a full CasSD domain and the broad distribution implying multiple intermediate states and the unfolding pathways of the CasSD domains. Similarly, the unfolding forces also showed a random and broad distribution, ranged from 30 to 160 pN (Fig. 3b), and no characteristic unfolding force was identified. Importantly, no correlation between ΔL and unfolding force was found.

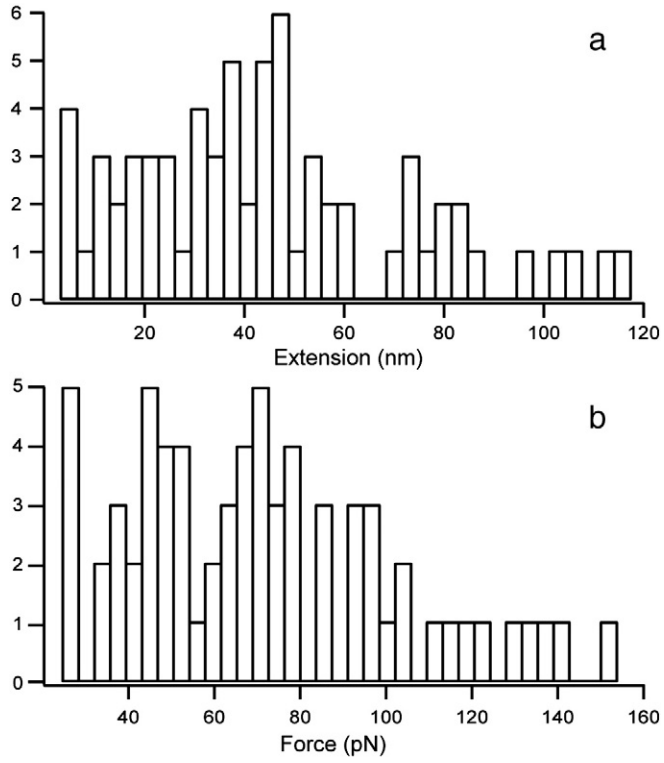

Fig. 3. Histograms of CasSD contour length change during unfolding (a) and unfolding force (b) retrieved from AFM experiment. Both datasets tend to be randomly dispersed over the range, instead of forming Gaussian-fitted peaks as usually observed in structured proteins.

3.2. Unfolding CasSD–fibronectin constructs at near equilibrium state

In above AFM experiments, the CasSD construct was stretched in a fast manner, results in unfolding forces usually much higher than 20 pN. In contrast, MT experiments can ramp the force very slowly (Fig. 4b, c) and reach a force regime much closer to physiological conditions *in vivo*, where the average mechanical force is estimated in the scale of a couple of pN [26]. At a force ramping rate of 0.01 ~ 0.1 pN/s, the unfolding forces of CasSD (Fig. 5) domains were lower than obtained above in AFM experiments, while a broad distribution of forces was also observed, ranged from 0.76 pN to 50 pN. However, unlike the random distributed unfolding forces from AFM experiments, a majority of unfolding events from MT took place at forces within a much smaller range. The histogram of unfolding forces from MT showed a population peak and was fitted by a Gaussian distribution centered at 4.96 pN with the width at half maximum of 8.8 pN. Here, non-feature unfolding of CasSD, as those measured in AFM pulling experiments, was not identified. This doesn't mean that those unfolding events didn't exist, because no feature of those unfolding events made them hard to be distinguished from failure measurements.

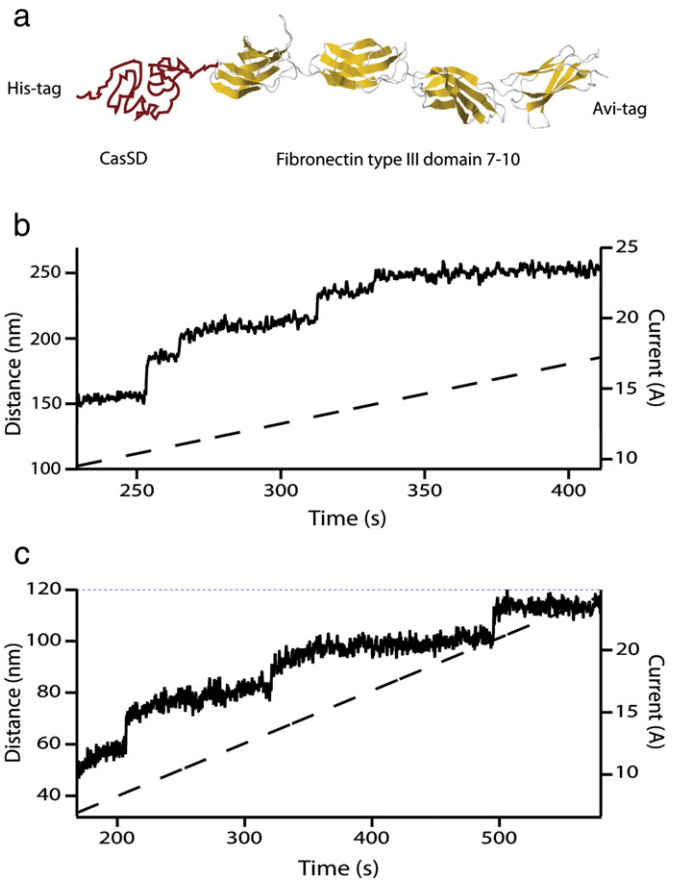

Fig. 4. Unfolding CasSD–fibronectin under magnetic tweezers. (a) A scheme of the His_6–CasSD–$FnIII_{7-10}$–Avi construct. Fibronectin works as a long linker for better suppression of non-specific interaction between magnetic bead and quartz surface. Typical unfolding trajectories under an upward force clamp are shown in (b) and (c). Each sudden increase in distance signifies unraveling of a protein structure.

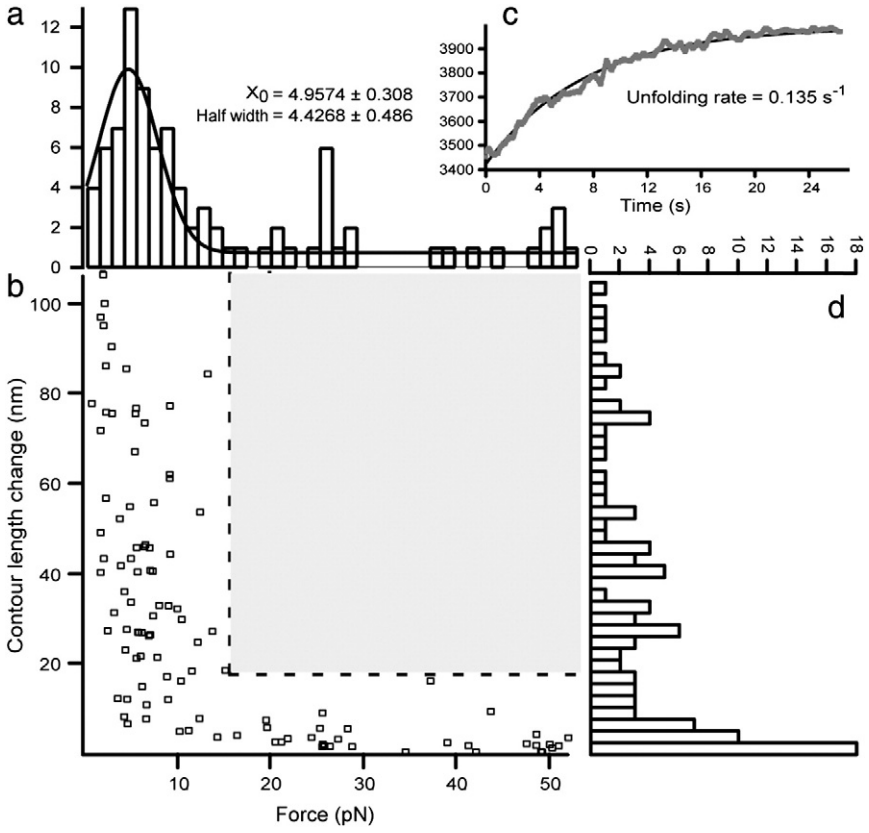

Fig. 5. CasSD contour length change upon unfolding versus unfolding force under magnetic tweezers. a) The histogram of unfolding forces, where a Gaussian fit gives a peak around 4.96 pN and a half width of the half maximum around 4.4 pN. b) The 2-dimensional graph of the contour lengths versus forces, showing the random interspersion of unfolding events on the contour length change/force plane. c) The dwell time analysis of CasSD unfolding events. Unfolding steps with known pre- and post-unfolding dwell time from CasSD unfolding trajectories under magnetic tweezers were chosen. Raw data associated with each such step and spanning both dwell time were aligned depending on time of course. Distance of all aligned mirror-image-of-Z-like curves were added up. The final curve was fitted with an exponential growth with an unfolding rate of 0.135 s^{-1}. d) The histogram of contour length changes, showing almost even distribution along the whole range up to the full contour length of the CasSD domain.

On the other hand, histogram of contour length change displays a rather evenly-distributed pattern. Interspersion of unfolding events on the force–Δ*L* plane (2D map in Fig. 5) reinforces such randomness.

It is also interesting to notice that, there is not any event associated with both unfolding force above 15 pN and step size larger than 16 nm. This blank area in the 2D map may suggest the following deduction: for interaction stabilizing CasSD native conformation, all long range interactions are rather weak whereas short range interactions span a broad force spectrum. Distribution of unfolding forces is most likely biased by the slow ramp mode we used, in which unfolding probability is a sigmoidal function of stretching force, making the shape of probability density function and histogram of force both bell-like [27,28].

Besides unfolding events, 13 refolding steps were observed in the ramping down experiment following the stretching (Fig. S3, Supplementary materials). Out of them, four events share contour length changes similar to prior corresponding unfolding steps, while the rest shows contour length change in a random fashion. Refolding events, though rarer to be observed, also implies a structural diversity of CasSD population, as already demonstrated by unfolding events (Supplementary materials).

3.3. Unfolding rates of CasSD in MT experiments

The period between any two successive CasSD unfolding events at near-equilibrium state varies by orders of magnitude. The lower limit of the observed dwell time was the time resolution of the camera system, 0.044 s, within which it is impossible to differentiate any two events occurring. Beginning with section of chosen dwell time, followed by the unfolding step and ending with a short flat segment of unfolded state, 29 such unfolding trajectories were aligned according to their time course and adjusted to same length by changing the extent of last segment. After adding up their contour lengths, resulting curve was fitted by an exponential function with a time constant $\tau = 7.41$ s, corresponding to an unfolding rate of 0.135 s^{-1} (insert, Fig. 5). To test how much the result was biased by the broad unfolding forces applied, all unfolding trajectories described above were divided into two groups depending on whether their unfolding force was larger than 10 pN. Analysis of both groups revealed unfolding rates of 0.131 and 0.13 s^{-1} respectively, nearly identical to each other and closed to 0.135 s^{-1} as well. Thus we believe our result should represent the true unfolding rate under constant force to a certain extent.

4. Discussions

4.1. CasSD is intrinsically disordered

AFM force spectroscopy is able to probe not only unfolding pathways of proteins but also their conformations, through the measurements of their responses and the contour length changes (Δ*L*) [29]. If the protein is natively folded and mechanically stable, unfolding events with characteristic Δ*L* and unfolding forces can be observed in AFM force measurements. However, this is not the case for CasSD. In our experiments, more than half of CasSD probed by AFM presented featureless response to stretching, indicating most likely random coil conformations. Though the rest of the trajectories of CasSD showed patterns of unfolding events, diverse Δ*L* and unfolding forces were observed, corresponding to varied stable conformations. Similar unfolding trajectories were also reported for α-synuclein, N2B isoform of cardiac I-band titin, VAMP2 and other PEVK region of

titin, while α-synuclein and N2B isoform are classified as ID proteins [30–33]. Thus, CasSD should also belong to the group of ID proteins.

For those ID proteins, AFM force–extension trajectories with some mechanical features were ascribed to α-helix, β-like structures or weak interactions, all of which are mechanically more stable than random coil. Our results indicate that CasSD might be a similar case. Nevertheless, it was also noticed that CasSD is a proline-rich domain, which could also take PPII helix conformations. Anyway, their random and broad unfolding behaviors suggest folded states contributed by various interactions between random points along the amino sequence.

The existence of these states was also confirmed by the result of magnetic tweezers experiment, where those conformations of CasSD other than random coils tended to be similar in mechanical stability. This is indicated by the preferred unfolding force under close-to-equilibrium stretching as well as the similar unfolding rates regardless of the stretching force applied. Thus, either those interactions stabilizing those conformations of CasSD are similar, or they are just weak and coincidently show similar strength. On the other hand, the unfolding contour length changes broadly distributed up to the contour length of the whole CasSD domain. Therefore, those interactions can be hydrophobic or electrostatic ones, or maybe even some weak interactions between the 15 YxxP motifs, where PPII helix may be formed, with varied lengths in between. Anyway, such interactions should be weak and dynamic; otherwise, the conformations of random coils could not dominate the distribution.

Though the majority conformations of random coils, the mechanical stability of CasSD in other conformations is significantly low. In AFM pulling experiments, unfolding forces of those trajectories with noticeable events are much smaller than mechanical stable proteins, e.g. ubiquitin and I27, when similar constant velocities of stretching were adopted [24,25]. Under near equilibrium stretching in MT experiments, the majority of unfolding forces are around 5 pN, which is lower than unfolding force, ~7.6 pN of calmodulin, 13 pN of protein L, and 19 pN of Rnase H at similar conditions [22,34,35]. It is obvious that these proteins are less resistant to stretching compared with most members in Bio-Molecule Stretching Database (BSDB) [36]. Unfolding rate provides another aspect for the same comparison. CasSD unfolding rate at low force, $\alpha(5\ \mathrm{pN}) \sim 0.131\ \mathrm{s}^{-1}$, is considerably larger than that of protein L which has $\alpha(13\ \mathrm{pN}) \sim 0.14\ \mathrm{s}^{-1}$, $\alpha(0\ \mathrm{pN}) \sim 0.067\ \mathrm{s}^{-1}$, Rnase H with $\alpha(0\ \mathrm{pN}) \sim 3 \times 10^{-4}\ \mathrm{s}^{-1}$, and E-cadherin with $\alpha(5\ \mathrm{pN}) \sim 0.027\ \mathrm{s}^{-1}$ [22,35,37], meaning even at low force CasSD is more susceptible to unfolding than above proteins. CasSD native structures are held by interactions of low strength, and it also leads to the conclusion that CasSD is intrinsically disordered as can be suggested by single-molecule force spectroscopy [38].

4.2. CasSD as force transducer

Over half of the residues in scaffold protein centering in cell signaling and functions are predicted to be intrinsically disordered [39]. As an ID protein, CasSD is also involved in signaling processes, especially mechano-transductions, where mechanical signals are converted to chemical signals by exposing phosphorylation sites upon unfolding [2]. How the disordered nature of CasSD connects with its mechano-transduction feature and other multiple functions triggers our great interest, and we hope that understanding the intrinsic disordered states can shed light on more details of cellular function and regulation of CasSD.

The 15 YxxP motifs of the CasSD can be phosphorylated by Abelson tyrosine kinase, c-Src or focal adhesion kinase, etc. depending on cell type and external stimuli [40]. For example, only motif 6–15 can be efficiently phosphorylated by Src [16]. Our results imply various native conformations of CasSD, which should affect the accessibility of each YxxP motif. Thus, this can be one of the reasons leading to different efficiencies of tyrosine phosphorylation by those kinases at different conditions. In turn, different signaling pathways are invoked. Importantly, most native conformations of CasSD are not very stable, many mechanical signals, such as forces and extensions of the F-actin, can readily shift the populations of the conformations and change the biochemical responses of CasSD.

PEVK domains of titin share great similarities with CasSD. They are all ID regions, able to be phosphorylated, involved in mechanical function, and composed of population of random coil and other conformations of some mechanical stability at same time. One significant discovery about the former was their change of mechanical elasticity due to different environments [41,42]. Upon stretching, an environment with higher ionic strength leads to lower persistence length and extensibility of ID proteins [43,44]. Similarly, the conformational equilibrium of α-synuclein shifts from random coil to β-sheets and α-synuclein becomes more resistant to mechanical force in presence of Cu^{2+} [30]. Such increments in ionic strength promote α-synuclein oligomerization which explains the cause of some neurological diseases [30], but destabilizes binding of PEVK to its partner protein F-actin [45]. Likewise, phosphorylation has also been shown to increase PEVK's stiffness [46–48]. This is reasonable as high ionic strength promotes interaction between hydrophobic residues and extra phosphoric group may regulate the surface charge distribution resulting in additional intra-molecular interactions. However, such change does not necessarily enhance interactions between IDP to its partners. Here we extend this mechanism to CasSD and speculate that it may undergo similar transformation in changing environment to regulate tyrosine phosphorylation and downstream signaling pathway. It also opens possibilities that actively modifying mechanical property of CasSD, making it more resistant to unravel, may stand for a novel technique to prevent metastasis of tumor cell, and a cure to other relative conditions.

Summary

In this study, we used AFM and MT to stretch CasSD domains. The results demonstrated that the native CasSD can take many conformations while the majority of them are random coils. This confirms its nature as an intrinsically disordered protein. Most of the native conformations of CasSD turned out to have limited mechanical resistance. Those non-random-coil conformations showed similar unfolding forces and unfolding rates indicating that they were stabilized by similar weak intramolecular interactions, which might be interactions between YxxP motifs. Nevertheless, CasSD was ready to be extended. Thus, instead of sensing forces, CasSD is more likely able to transform any mechanical extension associated into biochemical signals.

Acknowledgments

We gratefully acknowledge support from the Research Start Fund for Talent Recruitment, Chongqing University, China, and the seed grant (WBS R-714-002-007-271) from the Mechanobiology Institute, Singapore.

Appendix A. Supplementary data

Supplementary data to this article can be found online at http://dx.doi.org/10.1016/j.bpc.2013.06.008.

References

[1] M. Tamada, M.P. Sheetz, Y. Sawada, Activation of a signaling cascade by cytoskeleton stretch, Dev. Cell 7 (5) (2004) 709–718.
[2] Y. Sawada, et al., Force sensing by mechanical extension of the Src family kinase substrate p130Cas, Cell 127 (5) (2006) 1015–1026.
[3] D.M. Donato, et al., Dynamics and mechanism of p130Cas localization to focal adhesions, J. Biol. Chem. 285 (27) (2010) 20769–20779.

[4] H. Honda, et al., Cardiovascular anomaly, impaired actin bundling and resistance to Src-induced transformation in mice lacking p130Cas, Nat. Genet. 19 (4) (1998) 361–365.
[5] M. Auvinen, et al., Ornithine decarboxylase- and ras-induced cell transformations: reversal by protein tyrosine kinase inhibitors and role of pp130CAS, Mol. Cell. Biol. 15 (12) (1995) 6513–6525.
[6] S. Cabodi, et al., Integrin signalling adaptors: not only figurants in the cancer story, Nat. Rev. Cancer 10 (12) (2010) 858–870.
[7] M. Zhao, K. Vuori, The docking protein p130Cas regulates cell sensitivity to proteasome inhibition, BMC Biol. 9 (2011) 73.
[8] R. Janostiak, et al., Tyrosine phosphorylation within the SH3 domain regulates CAS subcellular localization, cell migration, and invasiveness, Mol. Biol. Cell 22 (22) (2011) 4256–4267.
[9] A. Brinkman, et al., BCAR1, a human homologue of the adapter protein p130Cas, and antiestrogen resistance in breast cancer cells, J. Natl. Cancer Inst. 92 (2) (2000) 112–120.
[10] P. Defilippi, P. Di Stefano, S. Cabodi, p130Cas: a versatile scaffold in signaling networks, Trends Cell Biol. 16 (5) (2006) 257–263.
[11] E. Brugnera, et al., Unconventional Rac-GEF activity is mediated through the Dock180-ELMO complex, Nat. Cell Biol. 4 (8) (2002) 574–582.
[12] A.H. Bouton, R.B. Riggins, P.J. Bruce-Staskal, Functions of the adapter protein Cas: signal convergence and the determination of cellular responses, Oncogene 20 (44) (2001) 6448–6458.
[13] G.M. O'Neill, S.J. Fashena, E.A. Golemis, Integrin signalling: a new Cas(t) of characters enters the stage, Trends Cell Biol. 10 (3) (2000) 111–119.
[14] S.Y. Cho, R.L. Klemke, Purification of pseudopodia from polarized cells reveals redistribution and activation of Rac through assembly of a CAS/Crk scaffold, J. Cell Biol. 156 (4) (2002) 725–736.
[15] R.L. Klemke, et al., CAS/Crk coupling serves as a "molecular switch" for induction of cell migration, J. Cell Biol. 140 (4) (1998) 961–972.
[16] N.Y. Shin, et al., Subsets of the major tyrosine phosphorylation sites in Crk-associated substrate (CAS) are sufficient to promote cell migration, J. Biol. Chem. 279 (37) (2004) 38331–38337.
[17] M.R. Burnham, et al., Regulation of c-SRC activity and function by the adapter protein CAS, Mol. Cell. Biol. 20 (16) (2000) 5865–5878.
[18] A. del Rio, et al., Stretching single talin rod molecules activates vinculin binding, Science 323 (5914) (2009) 638–641.
[19] R. Roy, S. Hohng, T. Ha, A practical guide to single-molecule FRET, Nat. Methods 5 (6) (2008) 507–516.
[20] M. Rief, et al., Reversible unfolding of individual titin immunoglobulin domains by AFM, Science 276 (5315) (1997) 1109–1112.
[21] T.E. Fisher, et al., The study of protein mechanics with the atomic force microscope, Trends Biochem. Sci. 24 (10) (1999) 379–384.
[22] R.C. Liu, et al., Mechanical characterization of protein L in the low-force regime by electromagnetic tweezers/evanescent nanometry, Biophys. J. 96 (9) (2009) 3810–3821.
[23] A.F. Oberhauser, et al., Single protein misfolding events captured by atomic force microscopy, Nat. Struct. Biol. 6 (11) (1999) 1025–1028.
[24] M. Carrion-Vazquez, et al., Mechanical and chemical unfolding of a single protein: a comparison, Proc. Natl. Acad. Sci. U. S. A. 96 (7) (1999) 3694–3699.
[25] M. Carrion-Vazquez, et al., The mechanical stability of ubiquitin is linkage dependent, Nat. Struct. Biol. 10 (9) (2003) 738–743.
[26] N. Borghi, et al., E-cadherin is under constitutive actomyosin-generated tension that is increased at cell–cell contacts upon externally applied stretch, Proc. Natl. Acad. Sci. U. S. A. 109 (31) (2012) 12568–12573.
[27] A.F. Oberhauser, et al., Stepwise unfolding of titin under force-clamp atomic force microscopy, Proc. Natl. Acad. Sci. U. S. A. 98 (2) (2001) 468–472.
[28] M. Schlierf, H. Li, J.M. Fernandez, The unfolding kinetics of ubiquitin captured with single-molecule force-clamp techniques, Proc. Natl. Acad. Sci. U. S. A. 101 (19) (2004) 7299–7304.
[29] H. Dietz, M. Rief, Protein structure by mechanical triangulation, Proc. Natl. Acad. Sci. U. S. A. 103 (5) (2006) 1244–1247.
[30] M. Sandal, et al., Conformational equilibria in monomeric alpha-synuclein at the single-molecule level, PLoS Biol. 6 (1) (2008) e6.
[31] H. Li, et al., Reverse engineering of the giant muscle protein titin, Nature 418 (6901) (2002) 998–1002.
[32] H. Li, et al., Multiple conformations of PEVK proteins detected by single-molecule techniques, Proc. Natl. Acad. Sci. U. S. A. 98 (19) (2001) 10682–10686.
[33] J. Oroz, R. Hervas, M. Carrion-Vazquez, Unequivocal single-molecule force spectroscopy of proteins by AFM using pFS vectors, Biophys. J. 102 (3) (2012) 682–690.
[34] J. Stigler, et al., The complex folding network of single calmodulin molecules, Science 334 (6055) (2011) 512–516.
[35] C. Cecconi, et al., Direct observation of the three-state folding of a single protein molecule, Science 309 (5743) (2005) 2057–2060.
[36] M. Sikora, et al., BSDB: the biomolecule stretching database, Nucleic Acids Res. 39 (2011) D443–D450, (Database issue).
[37] F. Wu, et al., Dynamics of E-cadherin Extracellular Domains: Partial Unfolding and Intermediate States, 2013 (submitted for publication).
[38] A.F. Oberhauser, M. Carrion-Vazquez, Mechanical biochemistry of proteins one molecule at a time, J. Biol. Chem. 283 (11) (2008) 6617–6621.
[39] A. Balazs, et al., High levels of structural disorder in scaffold proteins as exemplified by a novel neuronal protein, CASK-interactive protein1, FEBS J. 276 (14) (2009) 3744–3756.
[40] D.D. Tang, p130 Crk-associated substrate (CAS) in vascular smooth muscle, J. Cardiovasc. Pharmacol. Ther. 14 (2) (2009) 89–98.
[41] M.C. Leake, et al., The elasticity of single titin molecules using a two-bead optical tweezers assay, Biophys. J. 87 (2) (2004) 1112–1135.
[42] M.C. Leake, et al., Mechanical properties of cardiac titin's N2B-region by single-molecule atomic force spectroscopy, J. Struct. Biol. 155 (2) (2006) 263–272.
[43] A. Nagy, et al., Hierarchical extensibility in the PEVK domain of skeletal-muscle titin, Biophys. J. 89 (1) (2005) 329–336.
[44] J.G. Forbes, et al., Titin PEVK segment: charge-driven elasticity of the open and flexible polyampholyte, J. Muscle Res. Cell Motil. 26 (6–8) (2005) 291–301.
[45] R. Yamasaki, et al., Titin–actin interaction in mouse myocardium: passive tension modulation and its regulation by calcium/S100A1, Biophys. J. 81 (4) (2001) 2297–2313.
[46] B.R. Anderson, et al., The effects of PKCalpha phosphorylation on the extensibility of titin's PEVK element, J. Struct. Biol. 170 (2) (2010) 270–277.
[47] M. Kruger, W.A. Linke, Protein kinase-A phosphorylates titin in human heart muscle and reduces myofibrillar passive tension, J. Muscle Res. Cell Motil. 27 (5–7) (2006) 435–444.
[48] M. Kruger, et al., Protein kinase G modulates human myocardial passive stiffness by phosphorylation of the titin springs, Circ. Res. 104 (1) (2009) 87–94.